Using Heterogeneous Data of Multi Frequency Astronomy for Testing Physical Models of GRB Emission

© Elena Mazaeva © Alexei Pozanenko © Pavel Minaev
Space Research Institute,
Moscow, Russia
elena.mazaeva@phystech.edu apozanen@iki.rssi.ru minaevp@mail.ru

Abstract. We discuss the problem of data heterogeneity in the search and analysis of inhomogeneities in the light curves of gamma-ray bursts afterglow. We use well-sampled optical and X-ray light curves to find and identify deviations (inhomogeneities) from smooth power law decay of the light curve. We show, in particular that the duration of the inhomogeneities correlates with their peak time (relative to gamma-ray burst trigger) and the correlation is the same for all types of inhomogeneities. The study of inhomogeneities can give us the opportunity to understand the physics of the "central machine" of gamma-ray bursts, which is still far from understanding.

Keywords: multi-frequency astronomy, data heterogeneity, gamma-ray burst, afterglow, light curve, inhomogeneity.

1 Introduction

Several astrophysical objects are observed right across the full electromagnetic spectrum (from highly energetic gamma-rays to radio waves). Synchronous observations of them in different wavelengths represent “Multi-Frequency Astronomy” (MFA). Also, observations of astrophysical events not only in electromagnetic waves, but in other channels, such as gravitational waves, introduce “Multi-Messenger Astronomy” (MMA).

The time-domain multi-frequency observations allow estimation of the physical parameters and discovery of the new features of the astrophysical object or event and make analysis more complex as a consequence.

MFA and MMA play a significant role in the investigation of gamma-ray burst (GRB) phenomena. E.g., analysis of the multi-color optical and two-frequency radio observations showed that the GRB ejecta are collimated in a jet [1]. Due to MMA, a reliably connection was established between short GRB and the merging binary neutron stars [2].

GRBs have extragalactic origin [3] and associated with the core collapse of massive stars and the accretion into the resulting black hole (type II or long bursts) or with the merger of two neutron stars or black holes (type I or short bursts). GRBs have long lasting X-ray, optical, infrared, radio afterglows.

The work continues the investigation [4] and concerns the analysis of the time-domain multi-frequency data to search for and to investigate the inhomogeneities of well-sampled optical and X-ray afterglow light curves of several GRBs. The analysis is complicated in particular due to data heterogeneity (see Section 2).

In general, optical light curves of the gamma-ray bursts in the afterglow phase are described fairly well by smoothly broken-power law [5] with temporal indices in the range from -0.5 to -2.5[6]. However, for the many well sampled optical light curves after subtracting the host-galaxy component significant deviations (inhomogeneities) from the smoothly broken-power law are observed. So far there is no clear understanding of the physical processes whereby they are created. However, there are several physical models explaining inhomogeneities:

• Density-jump model [7, 8] suggests that the inhomogeneities are connected with the interaction of the fireball with moderate density enhancements in the ambient medium;

• Two-component jet model [9] with a narrow ultra-relativistic outflow and a wide but mildly relativistic ejection;

• Energy-injection model [10, 11] is the most reliable, when GRB fireball receives an additional energy injection from the central engine during the afterglow phase.

But each model does not explain all features of the inhomogeneities, especially at late stages of the afterglow (dozens of days).

2 Experiments and the problem of data heterogeneity

2.1 Gamma-rays

In the gamma-ray range (above 10 keV) many different experiments operate to investigate GRBs. Each instrument is unique and typically consists of detector and imaging segments.

Detectors in various experiments are made of different materials and consist of several large blocks or matrices of relatively small elements.

To the first category we can refer the scintillation and semiconductor detector blocks, working in the typical energy range of 10 keV – 10 MeV:

1. sodium iodide (NaI): Fermi/GBM [12] and GGC-Wind/Konus [13];
2. bismuth germanate (BGO): INTEGRAL/SPI-ACS [13] and Fermi/GBM [11];

Proceedings of the XX International Conference “Data Analytics and Management in Data Intensive Domains” (DAMDID/RCDL’2018), Moscow, Russia, October 9-12, 2018

3. cesium iodide (CsI):Vernov/RELEC [15];
4. reverse-electrode n-type Ge detectors: INTEGRAL/SPI [16] and RHESSI [17].

More energetic gamma-rays (above 10 MeV) are registered by pair-conversion telescopes (e.g., Fermi/LAT [18]).

In the soft gamma-ray range (15 – 200 keV) large-area solid state CdZnTe detector arrays (e.g., Swift/BAT [19]) or multilayer cadmium telluride (CdTe) matrix detectors (e.g., INTEGRAL/ISGRI [20] and NuSTAR [21]) are common.

As for imaging segment, in the gamma-ray range the coded mask is commonly used (e.g., Swift/BAT, INTEGRAL/SPI, INTEGRAL/IBIS), which defines geometrically the telescope's field of view. Images of the sky are reconstructed by decoding the detector shadowgram with the mask pattern. However, some gamma-telescopes do not maintain the coded mask and are omnidirectional (e.g. INTEGRAL/SPI-ACS, Fermi/GBM, GGC-Wind/Konus, CGRO/BATSE).

Electronics and software onboard the gamma-telescopes run in different modes. Some of the experiments allow photon-by-photon mode (Swift/BAT, Fermi/GBM, INTEGRAL/SPI, INTEGRAL/IBIS-ISGRI), while several instruments only provide binned light curve sin the single or several energy channels: e.g. the INTEGRAL/SPI-ACS is operating in the single energy channel 0.1 - 10 MeV with time resolution of 50 ms.

The energy range and spectral resolution also significantly differ for different types of detectors.

Thereby, the data obtained from different gamma-ray telescopes are heterogeneous and the joint analysis of these data is complicated.

2.2 X-rays

To date, the X-ray observations (above 0.1 keV) of GRBs are predominantly obtained by Swift/XRT, a focusing X-ray telescope operating in 0.2 - 10 keV energy range [22]. It was designed to measure the fluxes, spectra, and light curves of GRBs prompt emission and afterglow over a wide dynamic range.

Swift/XRT supports three (imaging, windowed an photon-counting) readout modes to extend the dynamic range and to reveal rapid variability expected from GRB afterglows and autonomously determines which readout mode to use.

INTEGRAL/JEM-X is operating in the photon-by-photon mode in the 3 – 35 keV energy range and uses coded aperture mask for imaging [23]. It has much lower sensitivity comparing with Swift/XRT, making the observations of the X-ray afterglows almost impossible.

But JEM-X is capable of registering the prompt phase of GRBs 'by chance' due to its large field of view (7.5 deg. in diameter), allowing the investigation of the GRB at the beginning of the prompt phase including searching for precursors (see, e.g. [24]). Swift/XRT starts the GRB observations with the delay of several dozens of seconds due to slewing of the spacecraft.

As the consequence Swift/XRT provides deep soft X-ray afterglow observations, but INTEGRAL/JEM-X provides the prompt phase observations, so the data obtained by both experiment are not equivalent but complementary.

2.3 Optical (ultraviolet + visible + infrared) range

In optical range, GRBs are observed by both space- and ground-based telescopes.

Swift/UVOT is space telescope, operating in the 170 - 600 nm bandwidths [22].

On the ground, gamma-ray bursts are observed by a large number of telescopes (or collaborations of telescopes) with mirror diameters from 20 cm to 10 meters (corresponding upper limits of the registered flux are from 15th to 26th magnitudes).

Some of the collaborations providing follow-up GRB observations in optic are IKI FUN (IKI Follow-Up Network) and International Scientific Optical Network (ISON) [25].

In the GRB optical observations wide-band filters in the Johnson-Cousins UBVRI system and the Sloan Digital Sky Survey ugriz system are commonly used. The UBVRI system's magnitude zero-points were set by defining Vega to have colours of zero. The sensitivity maximum of U-band is 366.3 nm, B-band - 436.1 nm, V-band - 544.8 nm, R-band - 640.7 nm, I-band - 798.0 nm. The Sloan Digital Sky Survey ugriz system is based on flux measurements that are calibrated in absolute units, namely spectral flux densities, with a zero-point of 3631 Jansky (Jy). The sensitivity maximum of u-band is 356.6 nm, g-band - 463.9 nm, r-band - 612.2 nm, i-band - 743.9 nm, z-band - 889.6 nm [26].

The R-band is the most used for GRBs observations due to significant galactic and extragalactic absorption at higher frequencies.

Optical raw data are formed by the detectors array such as charge-coupled device (CCD) and are represented as images. Because of the time variations of the CCD characteristics and of the telescope optics (e.g. dust accumulation) each individual run is reduced separately. However, in order to have a data set as homogeneous as possible, the data reduction strategy should be identical. In the optical range the brightness (energy flux) of the astrophysical objects is measured in stellar magnitudes.

3 Observations and data sample

We analyzed light curves of the GRB 030329, GRB 151027A, GRB 160131A, GRB 160227A and GRB 160625B in optical and X-ray range to find and identify deviations (inhomogeneities) from broken power law.

The optical data were obtained by Crimean Astrophysical Observatory (CrAO), Sayan Solar Observatory (Mondy), Tian Shan Astrophysical Observatory (TShAO), Maidanak High-Altitude Observatory, Abastumani Astrophysical Observatory (AbAO), Special Astrophysical Observatory (SAO), ISON-Kislovodsk, ISON-Khureltogoot, ISON-NM observatories and taken from GCN observation report

circulars[2]. Observations were performed with an R-band of Johnson-Cousins system (approx. 90% of the total number of observations) and Clear filter. The optical photometrical data reduction is based on IRAF[3] standard tasks (/noao/digiphot/apphot). Finally, we performed cross-calibration analysis of photometrical data obtained with Clear and R filters to minimize selection effects (convergence to R-band data).

Optical data of GRB 030329 and GRB 160625B were taken from [27, 28]. The X-ray afterglow data of GRB 030329 were obtained by Rossi-XTE and XMM-Newton [29] in 0.5–2 keV range, the X-ray light curves of other GRBs received by Swift/XRT[4] in range of 0.3–10 keV.

The optical and X-ray light curves of the analyzed GRBs are presented in Figure 1.

4 Extraction of inhomogeneities

The light curves of GRB 151027A, GRB 160131A and GRB 160625B were approximated by a smoothly broken power law (Beuermann function, see e.g. [5]):

$$F = F_0 \left[\left(\frac{t-t_0}{t_{br}} \right)^{\alpha\omega} + \left(\frac{t-t_0}{t_{br}} \right)^{\beta\omega} \right]^{-\frac{1}{\omega}} \quad (1)$$

where α, β are the early and late power law indices, t_{br} is time of jet-break, ω is the smoothing parameter. The parameters α, β, t_{br} were fitted, t_0 (time offset) and ω were fixed ($t_0 = 0$, w = 1, 2, 3, 5, 7).

In case of GRB 160227A we use single power law model (see the formula 2), as we have only data for the first day after the burst trigger, probably before a jet-break time for this burst

$$F = F_0 t^{\alpha} \quad (2)$$

The GRB 030329 was modelled by a sum of two Beuermann functions:

$$F = \sum_{i=1}^{2} F_{0_i} \left[\left(\frac{t}{t_{jb_i}} \right)^{\alpha_i\omega_i} + \left(\frac{t}{t_{jb_i}} \right)^{\beta_i\omega_i} \right]^{-\frac{1}{\omega_i}} \quad (3)$$

The inhomogeneities (groups of points with significant deviation from the power-law-like behaviour) in the optical light curve were excluded from the fitting procedure.

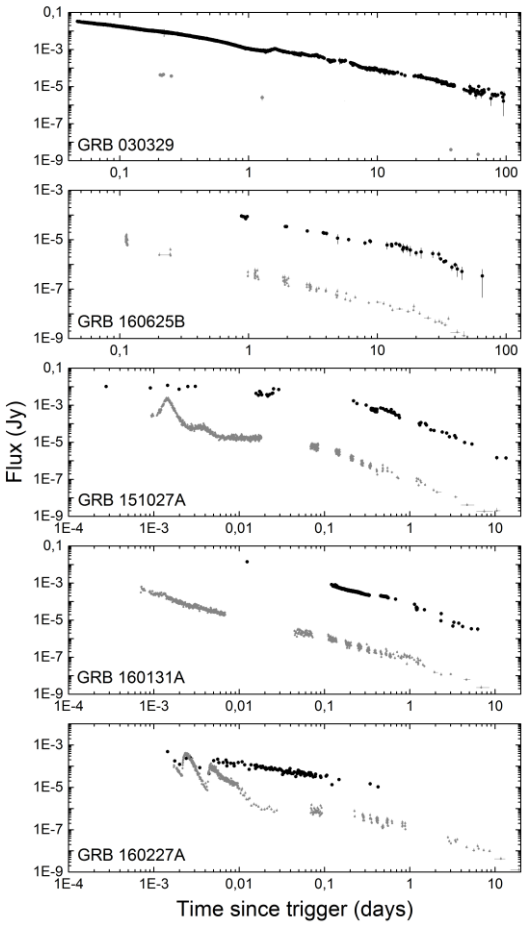

Figure 1 The optical (black) and X-ray (gray) light curves of the analyzed GRBs, expressed in Jy. X-ray band is 0.5–2 keV for GRB 030329 and 0.3–10 keV for other bursts. The host galaxy contribution was subtracted in the light curves of GRB 030329 and GRB 160625B.

5 Classification of inhomogeneities

The optical light curves reveal a number of inhomogeneities, superposed over the power-law decay (see Table 1). The inhomogeneities were approximated by polynomials.

We separate the inhomogeneities into several classes. The classification is following.

5.1 Flares

Flares (positive residuals) were found for the first time in the X-ray light curve of GRB 970508 [30, 31], later they have been observed in all phases of the canonical X-ray light curve [32].

In several GRB light curves, flares in X-ray and optical are synchronous. In our sample we found two such X-ray/optical flashes in GRB 151027A.

[2] https://gcn.gsfc.nasa.gov/gcn3 archive.html

[3] IRAF is distributed by the National Optical astronomy observatories.

[4] http://www.swift.ac.uk/xrt curves/

5.2 Bumps

Variations with positive residuals and without synchronous X-ray counterparts, we classified as the bumps.

5.3 Wiggles

Wave-like variations with transition from positive to negative (and vice versa) residuals and small amplitudes (several millimags) of the early afterglow (up to approximately 0.5 days since GRB trigger) were detected in a dense photometric data of GRB 030329 and GRB 160131A .

5.4 Nonclassified

Bumps with no synchronous detection in X-rays because of the absence of the corresponding X-ray data (like inhomogeneities of GRB 030329) or the inhomogeneities that do not fit the classification criteria are named as nonclassified. In particular, we could not classify the inhomogeneities of the GRB 160227A – the optical light curve has a complex structure with an additional component, which is not visible in X-rays.

Table 1 Fitted parameters of selected optical inhomogeneities

GRB	$T_{peak} - T_0$ (days)	FWHM (days)	Correlation with X-ray	Type [a]
030329	0.08826	0.03242	no data	W
030329	0.14657	0.04640	no data	W
030329	0.23522	0.08627	no data	W
030329	1.60190	0.24504	no data	n/c.
030329	2.62084	0.14206	no data	n/c.
030329	3.39444	0.41709	no data	n/c.
030329	3.61772	0.33584	no data	n/c.
030329	5.67352	1.15475	no data	n/c.
030329	8.79820	0.41162	no data	n/c.
030329	9.76593	0.37217	no data	n/c.
030329	10.76485	0.91008	no data	n/c.
030329	11.72378	0.65981	no data	n/c.
030329	12.58917	0.41100	no data	n/c.
151027A	0.53690	0.22988	yes	F
151027A	1.42918	0.25419	yes	F
151027A	2.66541	1.41120	no data	n/c.
160131A	0.16648	0.04802	no	W
160131A	0.24792	0.05253	no	W
160131A	0.16764	0.01142	no	B
160131A	0.52016	>0.05	no	B
160227A	0.00190	0.00078	yes	n/c.
160227A	0.00397	0.00145	yes	n/c.
160625B	14.44238	2.19765	no	B

[a] B — bump, F — flare, W — wiggle and n/c. — nonclassified inhomogeneities

7 The FWHM – T_{peak} relation

For derived parameters of FWHM and Tpeak we constructed scatterplot, presented in Figure 2. The optical flares detected by UVOT/Swift found in [32] are also plotted. For the UVOT sample only start and stop times of flashes are available, i.e. total duration of the flares. We use half of duration for each flash to put it on the Figure 3. The correlation between FWHM and T_{peak} found previously in [33] is evident. We fitted the FWHM - T_{peak} scatterplot for the combined sample using the power-law logarithmic model:

$$\log\left(\frac{FWHM}{1\ day}\right) = (1.05 \pm 0.03)\log\left(\frac{T_{peak}}{1\ day}\right) + (-0.86 \pm 0.07)$$

Power-law index of ~ 1 indicates the linear dependence of the investigated parameters: FWHM ~ T_{peak}. Earlier, the positive correlation between the arrival time and duration of X-ray flares was noted in [29].

It is interesting that all types of inhomogeneities introduced previously (wiggle, flare, bump, etc.) follow the same correlation (see Figure 3), possibly indicating their similar physical nature.

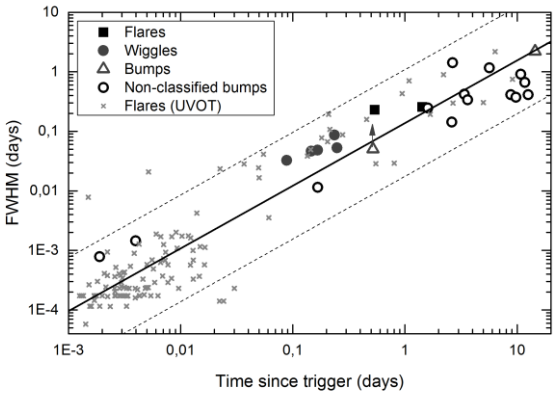

Figure 2 The FWHM – T_{peak} relation for inhomogeneities, constructed for ones from our sample and for flares detected by UVOT/Swift from [32]. Thick solid line represents power-law fit to the joint sample, dotted lines bound 2 sigma correlation region.

8 Discussion

In this paper, we analyzed the inhomogeneities of several GRB afterglow optical light curves. There are totally 23 inhomogeneities identified in five well sampled light curves. The inhomogeneities were classified as flares, bumps, wiggles and nonclassified.

The sample of 119 UV/optical flares from [32], mostly observed at early times (T_{peak} < 0.02 days) was jointly analyzed. We completed the sample by the late time inhomogeneities (21 at T_{peak} > 0.08 days).

All types of inhomogeneities from our sample and UVOT flares follow the same correlation between FWHM and T_{peak}, suggesting possible similar physical nature or strong selection effect. The power law index of the dependence is about 1 indicating a linear dependence of FWHM and T_{peak}.

Acknowledgments

The work was supported by the Russian Foundation for Basic Research (grant no. 17-51-44018).

References

[1] Harrison, F. A.; Bloom, J. S.; Frail, D. A.; Sari, R.; Kulkarni, S. R.; Djorgovski, S. G.; Axelrod, T. et al.: Optical and Radio Observations of the Afterglow from GRB 990510: Evidence for a Jet. In: The Astrophysical Journal, Volume 523, Issue 2, pp. L121-L124 (1999). doi: 10.1086/312282

[2] Abbott, B. P.; Abbott, R.; Abbott, T. D.; Acernese, F.; Ackley, K.; Adams, C.; Adams, T. et al.: Multi-messenger Observations of a Binary Neutron Star Merger. In: The Astrophysical Journal Letters, Volume 848, Issue 2, article id. L12, 59 pp. (2017). doi: 10.3847/2041-8213/aa91c9

[3] Meegan, C. A.; Fishman, G. J.; Wilson, R. B.; Paciesas, W. S.; Pendleton, G. N.; Horack, J. M.; Brock, M. N.; Kouveliotou, C.: Spatial distribution of gamma-ray bursts observed by BATSE. In: Nature (ISSN 0028-0836), vol. 355, p. 143-145 (1992). doi: 10.1038/355143a0

[4] Mazaeva, E., Pozanenko, A., Minaev, P.: Inhomogeneities in the light curves of gamma-ray bursts afterglow. In: International Journal of Modern Physics D, Vol. 27, 1844012 (2018). doi: 10.1142/S0218271818440121

[5] Beuermann, K.; Hessman, F. V.; Reinsch, K.; Nicklas, H.; Vreeswijk, P. M.; Galama, T. J.; Rol, E. et al.: VLT observations of GRB 990510 and its environment. In: Astronomy and Astrophysics, v.352, p.L26-L30 (1999).

[6] T. Krühler, Optical and near-infrared flares in GRB afterglows. In: Proc. Int. Astronomical Union, Conf. Death of Massive Stars: Supernovae and Gamma-Ray Bursts, 16 Vol. 352 (IAU Symposium, 2012), p. 46. doi: 10.1017/S1743921312012677

[7] Lazzati, D.; Rossi, E.; Covino, S.; Ghisellini, G.; Malesani, D.: The afterglow of GRB 021004: Surfing on density waves. In: Astronomy and Astrophysics, v.396, p.L5-L9 (2002). doi: 10.1051/0004-6361:20021618

[8] Dai, Z. G.; Wu, X. F.: GRB 030226 in a Density-Jump Medium. In: The Astrophysical Journal, Volume 591, Issue 1, pp. L21-L24 (2003). doi: 10.1086/377037

[9] Lamb, D. Q.; Donaghy, T. Q.; Graziani, C.: A Unified Jet Model of X-Ray Flashes, X-Ray-rich Gamma-Ray Bursts, and Gamma-Ray Bursts. I. Power-Law-shaped Universal and Top-Hat-shaped Variable Opening Angle Jet Models. In: The Astrophysical Journal, Volume 620, Issue 1, pp. 355-378 (2005). doi: 10.1086/426099

[10] Dai, Z. G.; Lu, T.: Gamma-ray burst afterglows and evolution of postburst fireballs with energy injection from strongly magnetic millisecond pulsars. In: Astronomy and Astrophysics, v.333, p.L87-L90 (1998).

[11] Zhang, Bing; Mészáros, Peter: Gamma-Ray Bursts with Continuous Energy Injection and Their Afterglow Signature. In: The Astrophysical Journal, Volume 566, Issue 2, pp. 712-722 (2002). doi: 10.1086/338247

[12] Meegan, Charles; Lichti, Giselher; Bhat, P. N.; Bissaldi, Elisabetta; Briggs, Michael S. et al.: The Fermi Gamma-ray Burst Monitor. In: The Astrophysical Journal, Volume 702, Issue 1, article id. 791-804, pp. (2009). doi: 10.1088/0004-637X/702/1/791

[13] Aptekar, R. L.; Frederiks, D. D.; Golenetskii, S. V.; Ilynskii, V. N.; Mazets, E. P. et al.: Konus-W Gamma-Ray Burst Experiment for the GGS Wind Spacecraft. In: Space Science Reviews, Volume 71, Issue 1-4, pp. 265-272 (1995). doi: 10.1007/BF00751332

[14] von Kienlin, A.; Beckmann, V.; Rau, A.; Arend, N.; Bennett, K. et al.: INTEGRAL Spectrometer SPI's GRB detection capabilities. GRBs detected inside SPI's FoV and with the anticoincidence system ACS. In: Astronomy and Astrophysics, v.411, p.L299-L305 (2003). doi: 10.1051/0004-6361:20031231

[15] Panasyuk, M. I.; Svertilov, S. I.; Bogomolov, V. V.; Garipov, G. K.; Balan, E. A.; Barinova, V. O.; Bogomolov, A. V. et al.: RELEC mission: Relativistic electron precipitation and TLE study on-board small spacecraft. In: Advances in Space Research, Volume 57, Issue 3, p. 835-849 (2016). doi: 10.1016/j.asr.2015.11.033

[16] Vedrenne, G.; Roques, J.-P.; Schönfelder, V.; Mandrou, P.; Lichti, G. G.; von Kienlin, A.; Cordier, B. et al.: SPI: The spectrometer aboard INTEGRAL. In: Astronomy and Astrophysics, v.411, p.L63-L70 (2003). doi: 10.1051/0004-6361:20031482

[17] Lin, R. P.; Dennis, B. R.; Hurford, G. J.; Smith, D. M.; Zehnder, A.; Harvey, P. R.; Curtis, D. W. et al.: The Reuven Ramaty High-Energy Solar Spectroscopic Imager (RHESSI). In: Solar Physics, v. 210, Issue 1, p. 3-32 (2002). doi: 10.1023/A:1022428818870

[18] Atwood, W. B.; Abdo, A. A.; Ackermann, M.; Althouse, W.; Anderson, B.; Axelsson, M.; Baldini, L. et al.: The Large Area Telescope on the Fermi Gamma-Ray Space Telescope Mission. In: The Astrophysical Journal, Volume 697, Issue 2, pp. 1071-1102 (2009). doi: 10.1088/0004-637X/697/2/1071

[19] Gehrels, N.; Chincarini, G.; Giommi, P.; Mason, K. O.; Nousek, J. A. et al.: The Swift Gamma-Ray Burst Mission. In: The Astrophysical Journal, Volume 611, Issue 2, pp. 1005-1020 (2004). doi: 10.1086/422091

[20] Ubertini, P.; Lebrun, F.; Di Cocco, G.; Bazzano, A.; Bird, A. J.; Broenstad, K.; Goldwurm, A. et al.: IBIS: The Imager on-board INTEGRAL. In:

Astronomy and Astrophysics, v.411, p.L131-L139 (2003). doi: 10.1051/0004-6361:20031173

[21] Harrison, Fiona A.; Craig, William W.; Christensen, Finn E.; Hailey, Charles J.; Zhang, William W.; Boggs, Steven E.; Stern, Daniel et al.: The Nuclear Spectroscopic Telescope Array (NuSTAR) High-energy X-Ray Mission. In: The Astrophysical Journal, Volume 770, Issue 2, article id. 103, 19 pp. (2013). doi: 10.1088/0004-637X/770/2/103

[22] Gehrels, N.; Chincarini, G.; Giommi, P.; Mason, K. O.; Nousek, J. A. et al.: The Swift Gamma-Ray Burst Mission. In: The Astrophysical Journal, Volume 611, Issue 2, pp. 1005-1020 (2004). doi: 10.1086/422091

[23] Lund, N.; Budtz-Jørgensen, C.; Westergaard, N. J.; Brandt, S.; Rasmussen, I. L.; Hornstrup, A.; Oxborrow, C. A. et al.: JEM-X: The X-ray monitor aboard INTEGRAL. In: Astronomy and Astrophysics, v.411, p.L231-L238 (2003). doi: 10.1051/0004-6361:20031358

[24] Minaev, P. Yu.; Grebenev, S. A.; Pozanenko, A. S.; Molkov, S. V.; Frederiks, D. D.; Golenetskii, S. V. : GRB 070912—A gamma-ray burst recorded from the direction to the galactic center. In: Astronomy Letters, Volume 38, Issue 10, pp.613-628 (2012). doi: 10.1134/S1063773712100064

[25] Pozanenko, A., Elenin, L., Litvinenko, E., Volnova, A., Erofeeva, A., Matkin, A., Ivanov, A. et al.: Gamma-ray burst observations with ISON network. In: Gamma-ray Bursts: 15 Years of GRB Afterglows. Edited by A. J. Castro-Tirado, J. Gorosabel, and I. H. Park. EAS Publications Series, Volume 61, pp.259-261 (2013). doi: 10.1051/eas/1361040

[26] Bessell, M. S.: Standard Photometric Systems. In: Annual Review of Astronomy & Astrophysics, vol. 43, Issue 1, pp.293-336 (2005). doi: 10.1146/annurev.astro.41.082801.100251

[27] Lipkin, Y. M.; Ofek, E. O.; Gal-Yam, A.; Leibowitz, E. M.; Poznanski, D.; Kaspi, S.; Polishook, D. et al. : The Detailed Optical Light Curve of GRB 030329. In: The Astrophysical Journal, Volume 606, Issue 1, pp. 381-394 (2004). doi: 10.1086/383000

[28] Zhang, B.-B.; Zhang, B.; Castro-Tirado, A. J.; Dai, Z. G.; Tam, P.-H. T.; Wang, X.-Y.; Hu, Y.-D. et al.: Transition from fireball to Poynting-flux-dominated outflow in the three-episode GRB 160625B. In: Nature Astronomy, Volume 2, p. 69-75 (2018). doi: 10.1038/s41550-017-0309-8

[29] Tiengo, A.; Mereghetti, S.; Ghisellini, G.; Tavecchio, F.; Ghirlanda, G.: Late evolution of the X-ray afterglow of GRB 030329. In: Astronomy and Astrophysics, v.423, p.861-865 (2004). doi: 10.1051/0004-6361:20041027

[30] Piro, L.; Amati, L.; Antonelli, L. A.; Butler, R. C.; Costa, E. et al.: Evidence for a late-time outburst of the X-ray afterglow of GB970508 from BeppoSAX. In: Astronomy and Astrophysics, v.331, p.L41-L44 (1998)

[31] Piro, L.; De Pasquale, M.; Soffitta, P.; Lazzati, D.; Amati, L. et al.: Probing the Environment in Gamma-Ray Bursts: The Case of an X-Ray Precursor, Afterglow Late Onset, and Wind Versus Constant Density Profile in GRB 011121 and GRB 011211. In: The Astrophysical Journal, Volume 623, Issue 1, pp. 314-324 (2005). doi: 10.1086/428377

[32] Swenson, C. A., Roming, P. W. A., De Pasquale, M. & Oates: Gamma-Ray Burst Flares: Ultraviolet/Optical Flaring. I. In: The Astrophysical Journal, Volume 774, Issue 1, article id. 2, 12 pp. (2013). doi: 10.1088/0004-637X/774/1/2

[33] Yi, Sh.-X., Yu, H., Wang, F. Y., Dai, Z.-G.: Statistical Distributions of Optical Flares from Gamma-Ray Bursts. In: The Astrophysical Journal, Volume 844, Issue 1, article id. 79, 8 pp. (2017). doi: 10.3847/1538-4357/aa7b7b